JACS
JOURNAL OF THE AMERICAN CHEMICAL SOCIETY

ARTICLE

pubs.acs.org/JACS

Soft Secondary Building Unit: Dynamic Bond Rearrangement on Multinuclear Core of Porous Coordination Polymers in Gas Media

Joobeom Seo,[†] Charlotte Bonneau,[†] Ryotaro Matsuda,[*,†,§,⊥] Masaki Takata,[∥,⊥] and Susumu Kitagawa[*,†,‡,§,⊥]

[†]ERATO Kitagawa Integrated Pores Project, Japan Science and Technology Agency (JST), Kyoto Research Park Bldg #3-405, Shimogyo-ku, Kyoto 600-8815, Japan

[‡]Department of Synthetic Chemistry and Biological Chemistry, Graduate School of Engineering, Kyoto University, Katsura, Nishikyo-ku, Kyoto 615-8510, Japan

[§]Institute for Integrated Cell-Materials Science (iCeMS), Kyoto University, Katsura, Nishikyo-ku, Kyoto 615-8510, Japan

[∥]Japan Synchrotron Radiation Research Institute/Spring-8, Sayo-gun, Hyogo 679-5198, Japan

[⊥]RIKEN Spring-8 Center, Sayo-gun, Hyogo 679-5198, Japan

Supporting Information

ABSTRACT: A new synthetic approach to prepare flexible porous coordination polymers (PCPs) by the use of soft secondary building units (SBUs) which can undergo multiple reversible metal−ligand bonds breaking is reported. We have prepared a zinc paddle-wheel-based two-fold interpenetrated PCP, $\{[Zn_2(tp)_2(\mathbf{L}^2)]\cdot 2.5DMF\cdot 0.5water\}_n$ (**2a**, H_2tp = terephthanlic acid; $\mathbf{L}^2$ = 2,3-difluoro-1,4-bis(4-pyridyl)benzene), showing dynamic structural transformations upon the removal and rebinding of guest molecules. The X-ray structures at different degrees of desolvation indicate the highly flexible nature of the framework. The framework deformations involve slippage of the layers and movement of the two interpenetrated frameworks with respect to each other. Interestingly, the coordination geometry of a zinc paddle-wheel unit (one of the popular SBUs) is considerably changed by bond breaking between zinc and oxygen atoms during the drying process. Two zinc atoms in the dried form **2d** reside in a distorted tetrahedral geometry. Compound **2d** has no void volume and favors the uptake of O_2 over Ar and N_2 at 77 K. The O_2 and Ar adsorption isotherms of **2d** show gate-opening-type adsorption behaviors corroborating the structure determination. The CO_2 adsorption isotherm at 195 K exhibits multiple steps originating from the flexibility of the framework. The structural transformations of the zinc clusters in the framework upon sorption of guest molecules are also characterized by Raman spectroscopy in which the characteristic bands corresponding to $\nu_{sym}(COO^-)$ vibration were used.

INTRODUCTION

Gas storage has become an industrial, economic, and environmental priority.[1,2] The last two decades have therefore witnessed dramatic efforts in the search for more efficient and adaptable solid gas adsorbents. Porous coordination polymers (PCPs) or Metal organic frameworks (MOFs), where properties of metal ions and functional organic ligands can be combined almost at will, are imposing themselves as a serious alternative to conventional zeolites and activated carbons.[3−18] Because adsorption properties are primarily bound to structure, the control over structure, which is achieved by synthesis, is crucial.[19−25] From the synthetic point of view, secondary building units (SBUs)[26] designed to produce directional polyatomic metal clusters have much advantage for the rational design of PCPs compared to mononuclear metal centers. On the other hand, from a flexible viewpoint, SBUs are usually limited to providing soft porosity[19,27−36] because each metal atom is mutually interconnected via small number of atoms in the SBU, which interferes in dynamic change of coordination geometry.[3−5] By soft porosity, we refer to sorption profiles generating features that reside outside the classical sorption classification,[37] such as large hysteretic sorption,[19,27] stepwise uptake,[19,28,29,36] and gate-opening phenomena[30,31] among others. These properties come from structural flexibility, which is strongly related to guest-dependent phenomena.

In this work, we focus on making porous materials presenting the properties of soft porosity by using a synthesis scheme inspired from the SBU approach. To achieve this goal, flexibility must originate from the SBUs, i.e. the steric/chemical environment of the metal clusters must be tuned, so that SBUs can undergo multiple reversible metal−ligand bond-breaking events to achieve soft porosity. We aim at creating soft SBUs that can regenerate. While the overall connectivity of the framework is maintained upon the reversible transformation of the SBU, the pore size, shape and volume are changed, showing soft porosity without degrading the stability of the material.

It has been reported that the zinc paddle-wheel, known as a popular SBU, can twist in jungle-gym-type compounds, where square grid carboxylate sheets are pillared by pyridyl ligands, however without any drastic bond rearrangement in the SBU.[38,39] Seen as a drawback, most studies aim at stiffening the SBU.[40−42] In this work, unlike any other, we aimed at morphing the zinc paddle-wheel into a soft SBU with regenerative properties. We found that pillaring by slim and long axial ligands ($\mathbf{L}^1$ = 1,4-bis(4-pyridyl)benzene; $\mathbf{L}^2$ = 2,3-difluoro-1,4-bis(4-pyridyl)benzene, Scheme 1) can allow reversible metal−ligand

Received: March 2, 2011
Published: May 09, 2011

bond-breaking/-formation with the zinc atoms being four- or six-coordinated for the soft SBU, and five-coordinated for the normal paddle-wheel. This has profound consequences on sorption properties. A thorough structural characterization conducted by single X-ray diffraction and in situ gas pressure-controlled powder X-ray diffraction and Raman spectroscopy is provided.

Scheme 1. L^1 and L^2

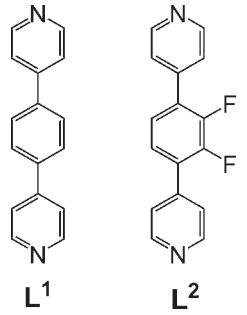

RESULTS AND DISCUSSION

Synthesis and Characterization of 1a and 1b. We first chose to synthesize a compound with the pillar L^1. Despite being successful in the synthesis of the compound and its crystal structure determination (**1a**, Figure 1a), its activated form (**1b**) while highly crystalline could not be characterized by single-crystal X-ray diffraction. In the view of the powder X-ray diffraction (PXRD) profiles, **1a** and **1b** could be entirely different phases (Figure 2) indicating that we might be successful in the obtention of a large distortion of the paddle-wheel. We proceeded to the thermogravimetric (TG) characterization and the measurement of sorption properties (Figures 3 and 4). The sorption for CO_2 shows an interesting multistep profile; however being deprived of the structure for **1b**, this study could not proceed any further. Compound **1a** and **1b** will be re-examined later in this paper.

Synthesis, Characterization, and Structural Transformations of 2a. We therefore moved on to an isostructural compound with another pillar L^2, for which we could obtain the structure of the activated form. It has been reported that fluorous MOFs can show enhanced stability.[43] The TG curve of the as-

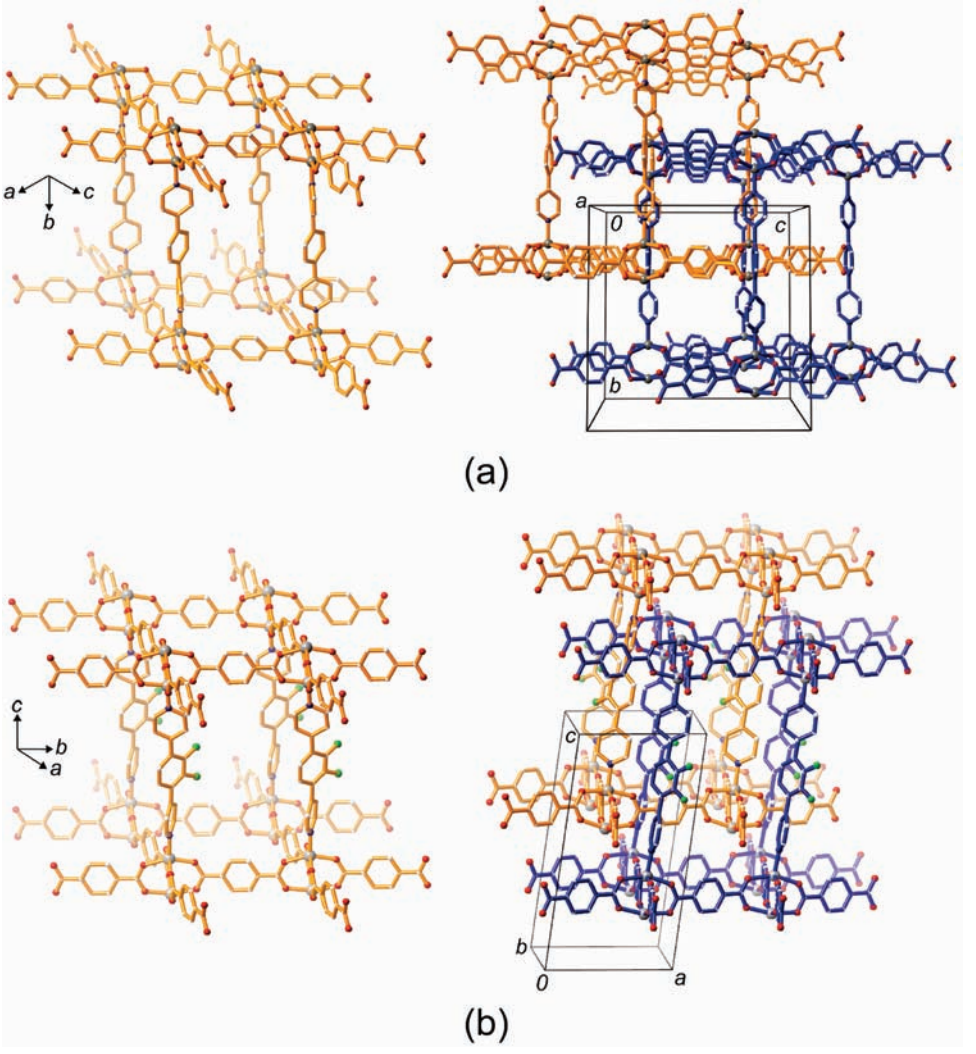

Figure 1. Crystal structures of (a) **1a** and (b) **2a**. From left to right: projection of the single framework and view of the two interpenetrated frameworks (orange and blue). Ball color: gray, zinc; blue, nitrogen; red, oxygen. Hydrogen atoms are omitted for clarity.

dx.doi.org/10.1021/ja201484s |*J. Am. Chem. Soc.* 2011, 133, 9005–9013

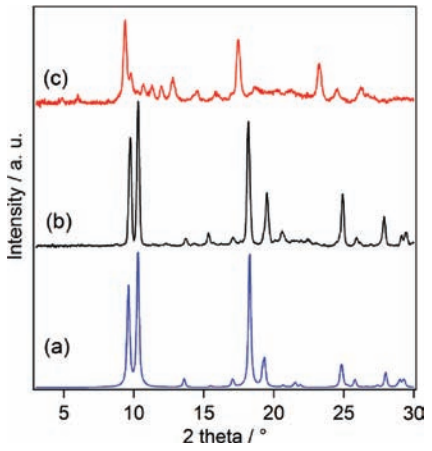

Figure 2. PXRD patterns of (a) simulation from single-crystal structure of **1a**, (b) the as-synthesized **1a**, and (c) drying of **1a** in vacuo at 388 K (**1b**). Data obtained using Cu *K*α radiation (λ = 1.54 Å).

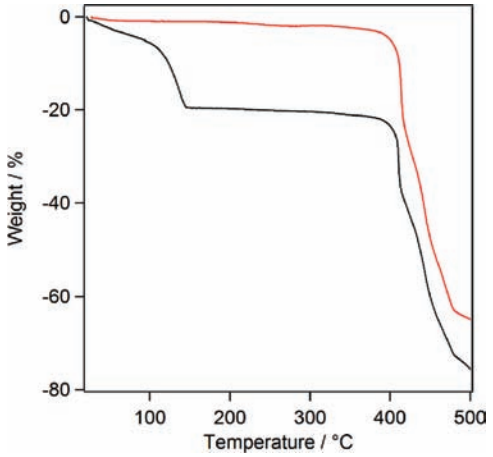

Figure 3. TGA profiles of the as-synthesized **1a** (black line) and the dried form **1b** (red line) with a heating rate of 5 K·min^{-1}.

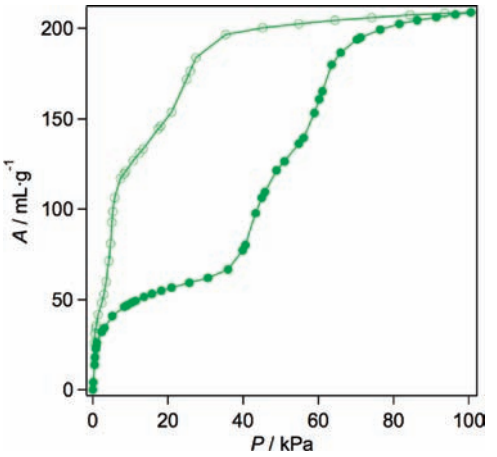

Figure 4. Adsorption (●) and desorption (○) isotherm of CO_2 at 195 K on **1b**. *A* is the amount adsorbed at standard temperature and pressure (STP).

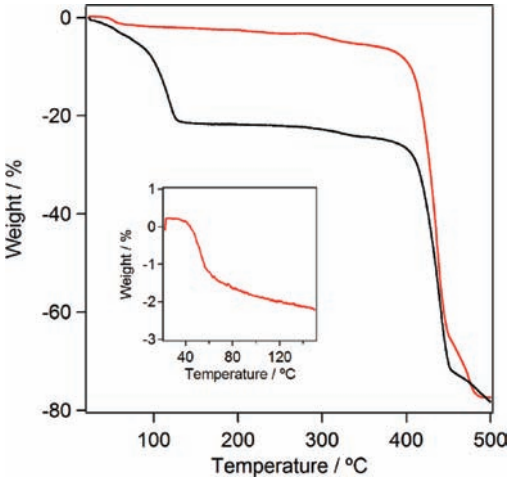

Figure 5. TGA profiles of the as-synthesized form **2a** (black line) and the dried form **2d** (red line) with a heating rate of 5 K· min^{-1}. (Inset) The TG curve of **2d** showing a 2.2% weight loss.

synthesized **2a** indicates the release of guest molecules up to 110 °C with a weight loss of 21.7% (calcd 22.0%) under an inert atmosphere (Figure 5). At 385 °C, the compound starts to break down being indicative of high thermal stability for this class of compounds. The TG curve of **2d** after handling in air shows a 2.2% weight loss (Figure 5 inset), which is equivalent to one water molecule per formula unit (calcd 2.4%).

The single-crystal X-ray structure determination of **2a** and **2d** shows two-fold interpenetrated 3D frameworks with the formula $\{[Zn_2(tp)_2(\mathbf{L^2})]\cdot 2.5DMF\cdot 0.5water\}_n$ and $[Zn_2(tp)_2(\mathbf{L^2})]_n$, respectively (Figures 1 and 6). While the triclinic $P\bar{1}$ space group and overall connectivity of the framework is preserved subsequently to the complete evacuation of the guests, two major structural changes of a different nature occur to lead to **2d**. First, the coordination environment of the zinc atoms is changed. In **2a**, the zinc ions are square pyramidal and arranged in the conventional paddle-wheel through bridged carboxylates. In stark contrast, in **2d** the zinc ions have become tetrahedral with one carboxylate out of two being monodentate; the paddle-wheel is transformed (Figure 6). The distance between zinc and oxygen atoms varies from 2.043(5) to 5.164 (14) Å for the cleaved bond; this is much larger than the sum of van der Waals radii (2.91 Å) (Figure 6 and Table 1). Hereafter, we call this configuration "open". Moreover, the open paddle-wheel provides an active metal site (Figure 6). The change in coordination mode of the carboxylate moieties presents characteristic Raman bands. The spectrum of **2a** shows double bands at around 1500 cm^{-1} and 1430 cm^{-1} corresponding to $\nu_{sym}(COO^-)$ vibrations of the normal zinc paddle-wheel, while a distinct single band at 1432 cm^{-1} is observed for **2d** (Figure 7). Second, as previously described for flexible two-fold interpenetrated pillared compounds, drastic reductions in cell volume (2070 to 1492 Å^3, 28%) and length of the *c*-axis (18.52 to 14.99 Å, 19%) can be observed from **2a** to **2d** (Table S1). These changes cause the single frameworks to move closer to each other (Figure S1). The structure of **2d** is nonporous (void volume determined using PLATON[48] is 6.5%). Because the amplitude of the global variations in the crystal structures is so large, it was anticipated that compound **2a** would go through several intermediate desolvated states.

To identify temperature transition thresholds, a variable temperature PXRD experiment of a bulk sample of **2a** from room temperature to 400 K was carried out (Figure 8). The variation of

dx.doi.org/10.1021/ja201484s |*J. Am. Chem. Soc.* 2011, 133, 9005–9013

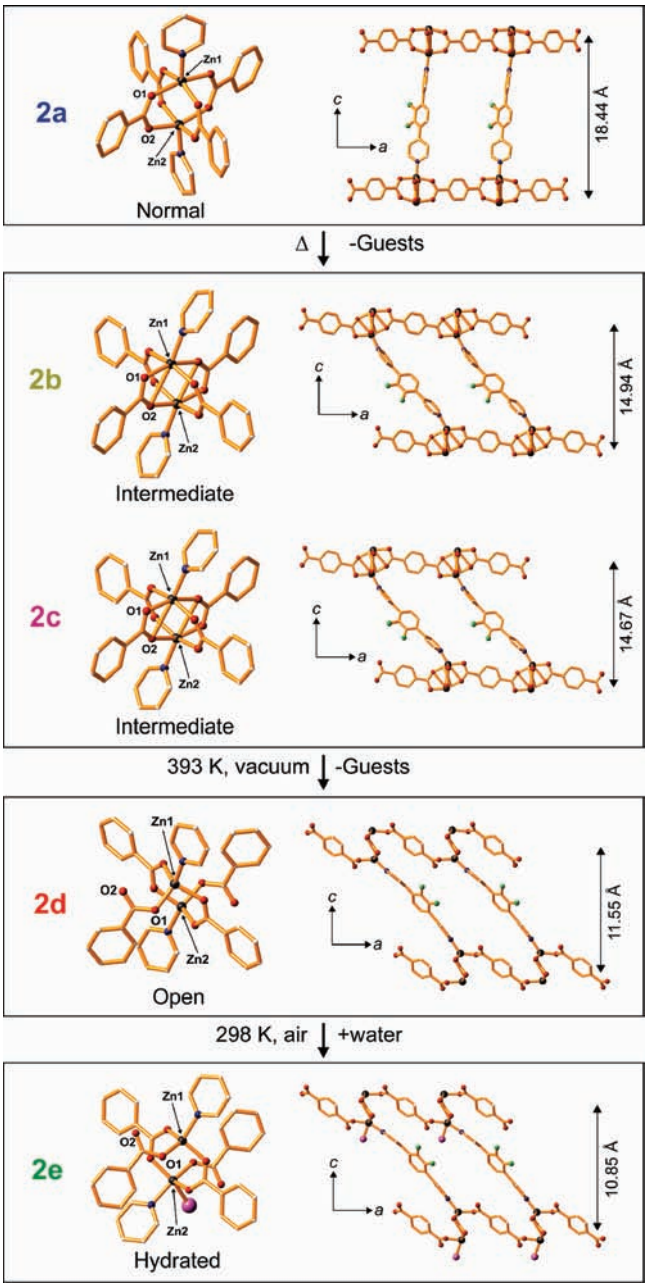

Figure 6. Crystal structure of **2a**, **2b**, **2c**, **2d**, and **2e** showing structural transformations upon desolvation and moisture coordination. Ball color: gray, zinc; green, fluorine; blue, nitrogen; red, oxygen; violet in **2e**, coordinated water. Noncoordinated guest molecules and hydrogen atoms are omitted for clarity. Coordination environments of the zinc cluster (left) and views of the single framework along the *b*-axis (right).

Table 1. Distance (Å) between Zinc and Oxygen Atoms of the Clusters

	2a	2b	2d
Zn1−O1	2.0208(8)	2.0387(4)	1.8884(5)
Zn2−O2	2.0343(5)	2.1283(6)	5.1639(14)

PXRD patterns showed that the structural transformations were gradual with no clear transition reaffirming the very soft behavior of the compound and none of the complex patterns could be indexed

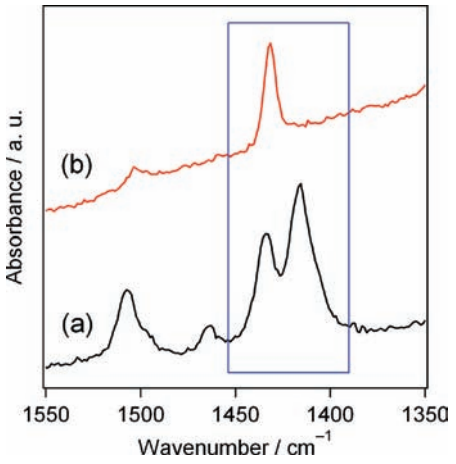

Figure 7. Raman spectra of (a) **2a** and (b) **2d**. The blue box indicates the band of $\nu_{sym}(COO^{-})$.

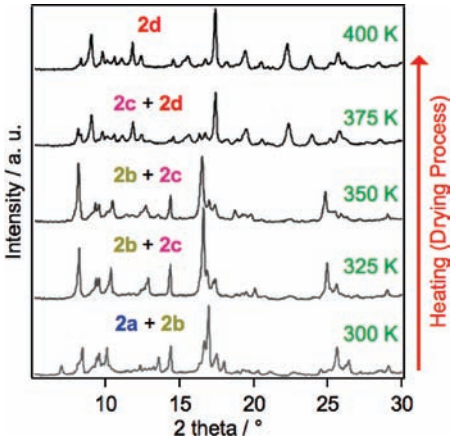

Figure 8. In situ PXRD patterns of the as-synthesized **2a** with increasing temperature, showing gradual structural transformations of **2a** upon drying process. Data obtained using Cu *K*α radiation (λ = 1.54 Å).

to a single phase. Nevertheless, the single-crystal structure determination of two intermediates (**2b** and **2c**) was obtained during the drying process (Figure 6). Although there are some unidentified peaks that may indicate coexistence of some unknown structures, the structures obtained enabled to discriminate most peaks and confirm the coexistence of at least two intermediates with different degrees of desolvation in the bulk sample (Figures S2 and S3). The framework connectivity and zinc coordination geometry of the intermediates are nearly identical, indicating that the transition of zinc cores to the open form requires complete desolvation. As anticipated from the TG experiment, the dried form **2d** with one open metal site is sensitive to air moisture; one water molecule coordinates readily to one of the zinc ions to give the hydrated form **2e**, $[Zn_2(tp)_2(\mathbf{L}^2)(H_2O)]_n$ (Figure 6). The Raman signature of **2e** is similar to that of **2d** with a single band at 1433 cm^{-1} (Figure S4). To ascertain the soft properties of the SBU, the reversibility of the transformations upon gas sorption must be confirmed.

Gas Sorption Properties of 2d. As compound **2d** has a nonporous structure, we expected that the sorption isotherms of **2d** would show gate-opening corresponding to the opening of the structure and/or a stepwise profile reflecting the formation of several structural intermediates. Gas adsorption isotherms were

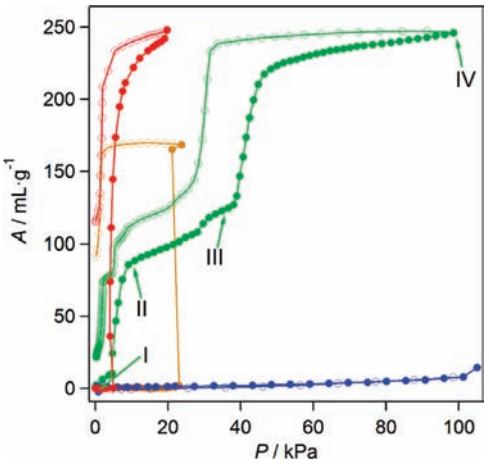

Figure 9. Adsorption (●) and desorption (○) isotherms of O_2 (77 K, red line), N_2 (77 K, blue line), Ar (77 K, yellow line) and CO_2 (195 K, green line) on **2d**. *A* is the amount adsorbed at STP.

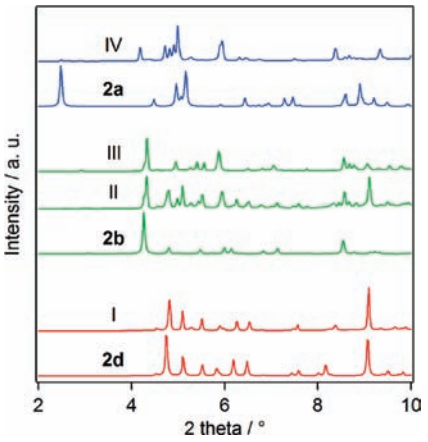

Figure 10. Comparisons of the simulated PXRD patterns of **2d** (dried form), **2b** (drying intermediate) and **2a** (as-synthesized form) and the observed PXRD patterns under 0 kPa (I), 10 kPa (II), 35 kPa (III) and 98 kPa (IV) of CO_2 at 195 K. Points I, II, III and IV are shown in Figure 9. Data obtained using synchrotron radiation (λ = 0.80 Å).

measured for N_2 (77 K), O_2 (77 K), Ar (77 K), and CO_2 (195 K). The adsorption isotherms show preferential uptake of O_2 over Ar and N_2 at 77 K (Figure 9). The O_2 and Ar adsorption isotherms are characterized by gate-opening-type adsorption, as expected from the nonporous structure of **2d**. The large differences in the onset pressures of similar gas molecules (5.0 kPa, P/P_0 = 0.25 for O_2 and 23.0 kPa, P/P_0 = 0.98 for Ar) at 77 K is important for the application in gas separation. We suppose that the preferential adsorption of O_2 could be attributed to a stronger interaction between guest and host molecule during the gate-opening process.[30−32,44−46] In contrast to the gate-opening-type adsorption isotherms for O_2 and Ar on **2d** at 77 K, the CO_2 adsorption isotherm at 195 K shows a stepwise sorption reflecting the framework flexibility. The fact that steps are not observed for O_2 and Ar does not indicate that the structure is rigid, but rather that the characterization of the framework flexibility by gas sorption is probe dependent. In details the CO_2 profile shows four steps: a first small step below 5 kPa, two intermediate steps up to 40 kPa, and a last one reaching the saturation of the compound.

Characterization of Structural Transformations of 2d upon Adsorption of CO_2 at 195 K. To understand the relationship between stepwise sorption and the structural transformations, we measured the PXRD patterns of **2d** at various vapor pressures of CO_2 corresponding to the different steps (Figure 10). The peak indexing of the pattern at P = 0 kPa confirmed the structure obtained from the single structure of **2d** (Table 2). The patterns obtained at P = 10 and 35 kPa cannot be indexed as single phases, indicative of the coexistence of several intermediate structures (Figures S5 and S6), which is in accord with the results obtained from the desolvation experiments (Figure 8) and with the low gradient uptake of the sorption profile in that region. Taking into account the results from the single-crystal study, we propose a set of unit cell parameters of the 35 kPa pattern (Table 2). This set of parameters fits all reflections, missing only three peaks belonging to the 0 kPa pattern (Figure S6). The fully CO_2 accommodated pattern could be successfully indexed accounting for all reflections (Table 2). The evolution of the unit cell parameters indicates that the structure of **2d** straightens gradually to become similar to those of the as-synthesized phase (**2a**) at CO_2 saturation. However, the difference in unit cell angles suggests that the fully CO_2-accommodated structure is somewhat different from that of **2a**, which is consistent with the observed deviation in the PXRD patterns (IV and **2a** in Figure 11). Given these results, we argue that the accommodation of CO_2 molecules in **2d** causes the reformation of the zinc paddle-wheel with a slightly different structure at saturation. To further support this hypothesis, and because PXRD data cannot provide information below 5 kPa due to the presence of mixtures under low CO_2 loading conditions, Raman spectroscopy measurements of **2d** were carried out in situ under CO_2 pressure from dried to fully saturated and back (Figure 11). As early as 16 kPa of CO_2 the characteristic double band of ν_{sym}-(COO^-) vibration around 1425 cm^{-1} appears, along with the band from the adsorbed CO_2 at 1374 cm^{-1} (Figure 11a).[47] The peak change indicates that the zinc paddle-wheel is reformed after the first step adsorption of CO_2 at 195 K. Increasing the pressure does not involve any further changes in the Raman vibrations apart from an increase in the intensity of the adsorbed CO_2 band. The spectra upon desorption are nearly a reverse mirror image of the spectra upon absorption (Figure 11b) in accord with the PXRD patterns measured under CO_2 sorption conditions (Figure S7). The sudden change of the $\nu_{sym}(COO^-)$ vibration band from 4.2 to 0 kPa of CO_2 upon desorption shows that the zinc paddle-wheel persists until the complete evacuation of CO_2 from the framework. The PXRD pattern measured at 0 kPa during the desorption conditions shows the restoration of **2d** after the evacuation of CO_2 from the framework (Figure S7). This is in accordance with single-crystal structural transformations of the as-synthesized framework (**2a**) upon desolvation (Figures 6 and S1). Considering that at 5 kPa, the geometries around zinc atoms are still tetrahedral, the uptake of CO_2 molecules might be eased by the open metal site in the very first step of the sorption, before experiencing a straightening of the structure accompanied by the reformation of the paddle-wheel, acting similarly to a gate-opening process. More importantly, the Raman spectroscopic study stands as a strong evidence to confirm the reversible metal−ligand bond formation of the paddle-wheel unit in **2d** induced by the accommodation of as few as two molecules per formula unit (16 kPa). From all the results acquired, we have demonstrated the fully reversible soft property of the zinc paddle-wheel.

Comparison of 1a and 2a. We decided to re-evaluate compound **1a** and its dried form **1b**. Because of the strong similarities

dx.doi.org/10.1021/ja201484s |*J. Am. Chem. Soc.* 2011, 133, 9005–9013

Table 2. Change of Lattice Parameters of 2d under Vapor Pressure of CO_2 at 195 K and Lattice Parameters of the As-Synthesized Form 2a

P (kPa)	a (Å)	b (Å)	c (Å)	α (deg)	β (deg)	γ (deg)	V (Å^3)	R_p	R_{wp}
0	9.7300(4)	10.4189(3)	14.8181(5)	98.055(3)	93.289(3)	101.591(4)	1451.37(9)	1.423	3.230
35	10.7927	10.8869	15.8976	83.377	98.813	98.839	1815.90	1.151	2.767
98	10.9568	10.9682	18.4159	91.153	94.255	90.434	2206.52	1.234	3.286
2a	10.885(2)	10.930(2)	18.518(4)	87.42(3)	84.99(3)	70.57(3)	2069.6(7)		

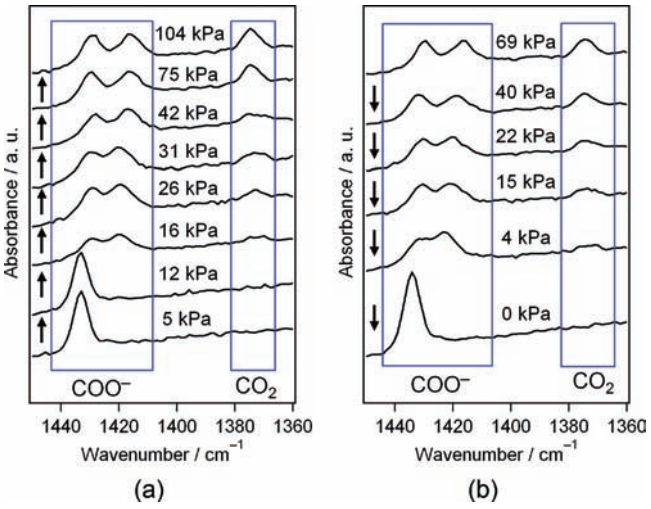

Figure 11. Raman spectra of **2d** upon (a) adsorption and (b) desorption of CO_2 at 195 K.

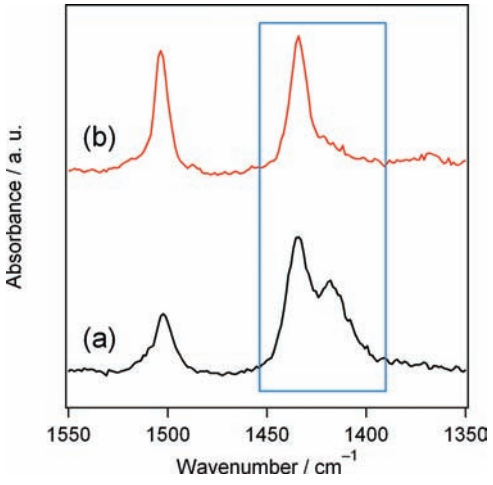

Figure 12. Raman Spectra of (a) **1a** and (b) **1b**. The blue box indicates the band of $\nu_{sym}(COO^-)$.

in the structure of **1a** and **2a** (Figure 1) and in the sorption profiles of their respective activated forms, **1b** and **2d**, this has lead us to speculate that **1b** is in fact isostructural to **2d** (Figure S8) and that its CO_2 sorption profile can be interpreted in similar terms as **2d**. As expected, **1a** shows the characteristic double band of the $\nu_{sym}(COO^-)$ vibration for the bridged carboxylates, while **1b** indicates the single band for the open paddle-wheel (Figure 12). In addition, the Raman spectral changes of **1b** under pressure of CO_2 at 195 K shows the reversible soft behavior of the zinc paddle-wheel, as characterized by the changes of the $\nu_{sym}(COO^-)$ vibration

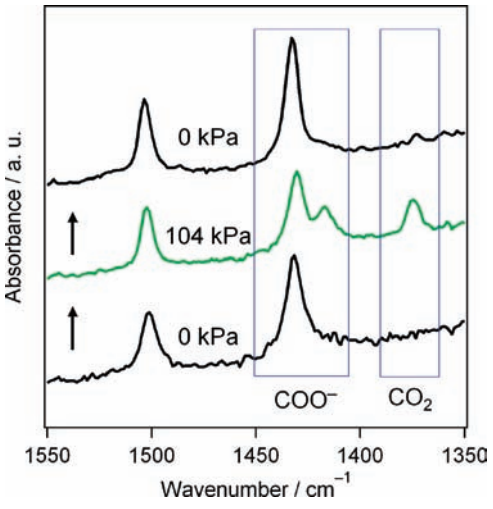

Figure 13. Raman spectral changes of **1b** upon adsorption and desorption of CO_2 at 195 K. The values on the spectra represent the vapor pressures of CO_2.

band (Figure 13). The use of the ligand $\mathbf{L^1}$ also allows the paddle-wheel to undergo severe distortions.

CONCLUSIONS

With the synthesis and characterization of the compounds reported above, besides providing extensive experimental evidence of the interplay between structure and multistep gas sorption, we have demonstrated that with a proper functionalization of the environment of a usually rigid SBU, we can modify its behavior so that it can reversibly flex to confer soft porous properties to a material. Furthermore, we gave the first account of the regeneration of the zinc paddle-wheel from its open form driven by the adsorption of a few gas molecules, showing that it is a low energy process and at the same time excluding any arguments about a possible recrystallization phenomenon in a solvated media. The development of porous compounds bearing soft SBUs expands further the possibilities of PCPs to be used as sophisticated gas adsorbents.

EXPERIMENTAL SECTION

General Methods. All chemicals and solvents used in the syntheses were of reagent grade and were used without further purification. Microwave reactions were performed using an Initiator 2.5 microwave from Biotage. The ^1H and ^{13}C NMR spectra were recorded with a JEOL JNM-ECS400 (400 MHz) NMR spectrometer. HRMS was obtained on a JEOL JMS-700 spectrometer. The elemental analysis was carried out on a Flash EA 1112 series, Thermo Finnigan instrument. The powder X-ray diffractions (PXRDs) were recorded with a RIGAKU UltimaIV or a Bruker D8 Discover diffractometer with GADDS equipped with

Scheme 2. Synthesis of L^2

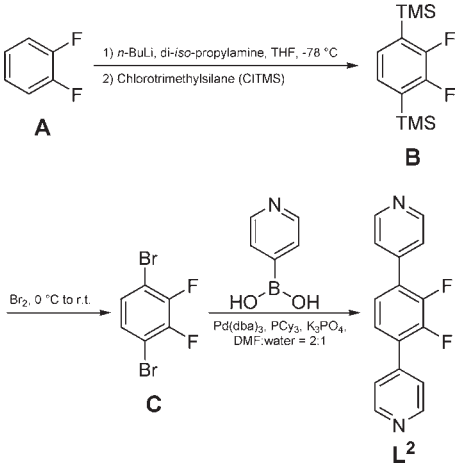

graphite monochromated Cu $K\alpha$ radiation (λ = 1.54073 Å). Thermogravimetric analyses were recorded on a Rigaku Thermo plus TG-8120 apparatus in the temperature range between 298 and 773 K at a heating rate of 5 K·min^{-1}. The Raman spectroscopy was carried out using a Horiba LabRAM HR-800 apparatus. A 785-nm laser was used for the excitation source. The slit width of the collection aperture was kept at 100 μm. All spectra were obtained in extended scan mode in the range of 50−3500 cm^{-1}. Calibration of the laser was performed in static scan mode using a silicon standard. The void volumes of crystal structures were estimated by PLATON.[48]

Preparation of $\{[Zn_2(tp)_2(L^1)]\cdot 2DMF\cdot 0.5water\}_n$ (1a) and $[Zn_2(tp)_2(L^1)]_n$ (1b). 1,4-Bis(4-pyridyl)benzene (L^1) was synthesized according to the literature method.[49] $Zn(NO_3)_2\cdot 6H_2O$ (29.7 mg, 0.10 mmol), terephthalic acid (16.6 mg, 0.10 mmol) and L^1 (11.6 mg, 0.05 mmol) were added in 3 mL of DMF. The tube containing the reaction mixture was sealed with an aluminum crimp cap fitted with a silicon septum and then exposed to microwave irradiation for 30 min at 115 °C. After cooling to room temperature, the resulting white solid (**1a**) was isolated by centrifugation and washed with DMF. The resulting white solid **1a** was heated to 115 °C under vacuum for 6 h to produce **1b**. Elemental analysis (%) calcd for **1b**·H_2O, $C_{32}H_{22}N_2O_9Zn_2$: C, 54.18; H, 3.13; N, 3.95. Found: C, 54.41; H, 3.14; N, 3.95.

Synthesis and Characterization of 2,3-Difluoro-1,4-bis-(trimethylsilyl)benzene (B) (Scheme 2). *n*-butyllithium (1.6 M in *n*-hexane, 5.7 mL, 40.3 mmol) was added to a solution of di-*iso*-propylamine (5.7 mL, 40.3 mmol) in anhydrous THF (20 mL) at −78 °C. After stirring 30 min at −78 °C, 1,2-difluorobenzene (**A**) (1.7 mL, 17.5 mmol) and chlorotrimethylsilane (4.9 mL, 38.5 mmol) was added to the solution at a rate which allowed the internal reaction temperature to remain below −50 °C. The solution was stirred at −78 °C for an additional 1 h. 1 M H_2SO_4 solution (10 mL) was added and then extracted with diethyl ether (20 mL × 3). The combined organic layers were washed with brine, dried over $MgSO_4$, and concentrated under reduced pressure to afford colorless needle-shaped crystals of **B** (4.47 g, 17.3 mmol, 98.8%). ^{1}H NMR ($CDCl_3$): δ 7.09 (*s*, 2H), 0.32 (*s*, 18H). LRMS (EI): m/z = 258 (M^+).

Synthesis and Characterization of 2,3-Difluoro-1,4-dibromobenzene (C) (Scheme 2). To a neat bromine (2.3 mL, 43.8 mmol) cooled to 0 °C was added portion wise solid **B** (3.78 g, 14.6 mmol) while maintaining the internal temperature between 20 and 40 °C. The reaction mixture was stirred at 58 °C for 2 h. After 1 h of this period had elapsed, additional bromine (0.4 mL, 7.30 mmol) was added. The reaction mixture was cooled to 0 °C and slowly poured into ice-cold saturated $NaHCO_3$ solution and extracted with diethyl ether (50 mL × 3). The combined organic layers were washed with brine, dried over $MgSO_4$, and concentrated under reduced pressure to afford colorless liquid **C**. The product was directly used for the following Suzuki coupling reaction without purification. ^{1}H NMR ($CDCl_3$): δ 7.23 (*m*, 2H). LRMS (EI): m/z = 272 (M^+).

Synthesis and Characterization of 2,3-Difluoro-1,4-bis(4-pyridyl)benzene (L^2) (Scheme 2). 2,3-Difluoro-1,4-dibromobenzene (**C**) (0.80 g, 2.94 mmol), 4-pyridineboronic acid (0.80 g, 6.47 mmol), potassium phosphate (5.50 g, 25.9 mmol), tris(dibenzylideneacetone)dipalladium (29.6 mg, 0.03 mmol), and tricyclohexylphosphine (25.2 mg, 0.09 mmol) were added in a mixture of dimethylformamide (10 mL) and water (5 mL). The tube containing the reaction mixture was sealed with an aluminum crimp cap fitted with a silicon septum and then exposed to microwave irradiation for 1 h at 150 °C. After cooling to room temperature, the reaction mixture was poured into water (50 mL) and extracted with dichloromethane (30 mL × 3), and the combined organic phases were washed three times with water. The solution was then dried over Na_2SO_4 and concentrated under reduced pressure. The residue was purified by recrystallization from dichloromethane as a white solid (0.27 g, 1.00 mmol, 35.0% based on **C**). ^{1}H NMR ($CDCl_3$): δ 8.74 (d, J = 6.0 Hz, 4H), 7.55 (d, J = 6.0 Hz, 4H), 7.37 (d, J = 4.1 Hz, 2H). ^{13}C NMR ($CDCl_3$): δ 150.39, 148.87 (dd, J_{CF} = 254, 16.0 Hz), 141.87, 128.66 (dd, J_{CF} = 7.0, 3.8 Hz), 124.86, 123.36. HRMS (EI) m/z calcd for $C_{16}H_{10}N_2F_2$ (M^+), 268.0812; found, 268.0802.

Preparation of $\{[Zn_2(tp)_2(L^2)]\cdot 2.5DMF\cdot 0.5water\}_n$ (2a) and $[Zn_2(tp)_2(L^2)]_n$ (2d). A solution of $Zn(NO_3)_2\cdot 6H_2O$ (29.7 mg, 0.10 mmol), terephthalic acid (16.6 mg, 0.10 mmol), and L^2 (13.4 mg, 0.05 mmol) in 3 mL of DMF was heated to 115 °C for 48 h to yield block-shaped colorless crystals of **2a**. Crystals were separated and washed with DMF and dried. The crystals of **2a** were heated to 115 °C under vacuum for 6 h to produce **2d**. Elemental analysis (%) calcd for **2d**·H_2O (**2e**), $C_{32}H_{20}F_2N_2O_9Zn_2$: C, 51.57; H, 2.70; N, 3.76. Found: C, 50.99; H, 2.75; N, 3.72.

Gas Adsorption Measurements. The sorption isotherm measurements were performed with the use of an automatic volumetric adsorption apparatus (BELSORP-18Plus or BELSORP-max; Bel Japan, Inc.). The dried sample was placed into the sample tube and then, prior to measurement, was evacuated again using the degas function of the analyzer for 3 h at 388 K. The change of the pressure was monitored and the degree of adsorption was detected by the decrease of the pressure at the equilibrium state. Highly pure gases (>99.999%) were used for the measurements.

X-ray Studies. Data were collected on Rigaku/MSC Saturn CCD diffractometer with confocal monochromated Mo$K\alpha$ radiation (λ = 0.7107 Å) and processed using the CrystalClear program (Rigaku). All the single-crystal structures were solved by direct methods and refined by full matrix least-squares refinement cycles on F^2 for all data using the SHELX-97.[50] The crystallizing solvents in **1a** and **2b** were disordered and could not be satisfactorily localized. Therefore, after all of the framework atoms (that were readily obtained from difference Fourier maps) were refined, the SQUEEZE[48] function was used to determine the contribution of the disordered solvent molecules that could not be refined to the structure factors. The contribution of these species was removed from the final structure factor calculations. The indistinguishable C and N atoms of the disordered DMF molecule in **2a** were refined by EXYZ and EADP constraints. The single crystals of **2b** were obtained by ex situ heating the single crystals of **2a** at 100 °C under N_2 atmosphere for 1 day. The single-crystal structure of **2c** was obtained by in situ heating of the crystals of **2a** from 25 to 80 °C with a heating rate of 1 K·min^{-1} for 55 min on a goniometer head. The crystals were heated for an addition 30 min at 80 °C, and then the crystals were cooled to −180 °C prior to the data collection. The diffraction data of the single crystal of **2d** were collected under continuous heating at 105 °C

dx.doi.org/10.1021/ja201484s |*J. Am. Chem. Soc.* 2011, 133, 9005–9013

using an N_2 stream to avoid the coordination of atmospheric water. Hydrogen atoms were placed in calculated positions.

Synchrotron Powder X-ray Diffraction Measurement and Analysis. PXRD patterns of **2d** under various vapor pressures of CO_2 were collected at SPring-8 (BL44B2)[51] with the synchrotron radiation (λ = 0.799640(2) Å). Before the data collections, sample of the dried form **2d** was put in a silica glass capillary and evacuated again under vacuum at 388 K for 1 h. After the evacuation, the sample **2d** was cooled down at 195 K under vacuum and high purity CO_2 gas was introduced at 10 kPa, 35 and 98 kPa. Le Bail analyses were done with the Rietica program.[52]

■ ASSOCIATED CONTENT

Supporting Information. Crystal data and structural refinement for **1a**, **2a**, **2b**, **2c**, **2d**, and **2e**, comparisons of PXRDs, and Raman spectrum of **2e**. These materials are available free of charge via the Internet at http://pubs.acs.org.

■ AUTHOR INFORMATION

Corresponding Author
ryotato.matsuda@kip.jst.go.jp; kitagawa@icems.kyoto-u.ac.jp

■ ACKNOWLEDGMENT

We thank Prof. Dr. Junliang Sun from Stockholm University for providing the lattice parameters obtained from powder diffraction data, and also thank Dr. K. Kato from RIKEN for his help for the synchrotron powder X-ray measurements. The synchrotron radiation experiments were performed at BL44B2 in SPring-8 with the approval of RIKEN (Proposal No. 20100061).

■ REFERENCES

(1) Davis, M. E. *Nature* **2001**, *417*, 813.
(2) Morris, R. E.; Wheatley, P. S. *Angew. Chem., Int. Ed.* **2008**, *47*, 4966.
(3) Dietzel, P. D. C.; Besikiotis, V.; Blom, R. *J. Mater. Chem.* **2009**, *19*, 7362.
(4) Klein, N.; Senkovska, I.; Gedrich, K.; Stoeck, U.; Henschel, A.; Mueller, U.; Kaskel, S. *Angew. Chem., Int. Ed.* **2009**, *48*, 9954.
(5) Yaghi, O. M.; O'Keeffe, M.; Ockwig, N. W.; Chae, H. K.; Eddaoudi, M.; Kim, J. *Nature* **2003**, *423*, 705.
(6) Bradshaw, D.; Claridge, J. B.; Cussen, E. J.; Prior, T. J.; Rosseinsky, M. J. *Acc. Chem. Res.* **2005**, *38*, 273.
(7) Férey, G.; Serre, C. *Chem. Soc. Rev.* **2008**, *38*, 1380.
(8) Kitagawa, S.; Kitaura, R.; Noro, S.-i. *Angew. Chem., Int. Ed.* **2004**, *43*, 2334.
(9) Li, J.-R.; Kuppler, R. J.; Zhou, H.-C. *Chem. Soc. Rev.* **2009**, *38*, 1477.
(10) Murray, L. J.; Dincă, M.; Long, J. R. *Chem. Soc. Rev.* **2009**, *38*, 1294.
(11) Shimizu, G. K. H.; Vaidhyanathan, R.; Taylor, J. M. *Chem. Soc. Rev.* **2009**, *38*, 1430.
(12) Suh, M. P.; Cheon, Y. E.; Lee, E. Y. *Coord. Chem. Rev.* **2008**, *252*, 1007.
(13) Banerjee, R.; Phan, A.; Wang, B.; Knobler, C.; Furukawa, H.; O'Keeffe, M.; Yaghi, O. M. *Science* **2008**, *319*, 939.
(14) Kawamichi, T.; Haneda, T.; Kawano, M.; Fujita, M. *Nature* **2009**, *461*, 633.
(15) Ma, L.; Falkowski, J. M.; Abney, C.; Lin, W. *Nature Chem.* **2010**, *2*, 838.
(16) Tan, J. C.; Bennett, T. D.; Cheetham, A. K. *Proc. Natl. Acad. Sci. U.S.A.* **2010**, *107*, 9938.
(17) Wang, Z.; Cohen, S. M. *Chem. Soc. Rev.* **2009**, *38*, 1315.
(18) Kishan, M. R.; Tian, J.; Thallapally, P. K.; Fernandez, C. A.; Dalgarno, S. J.; Warren, J. E.; McGrail, B. P.; Atwood, J. L. *Chem. Commun.* **2010**, *46*, 538.
(19) Seo, J.; Matsuda, R.; Sakamoto, H.; Bonneau, C.; Kitagawa, S. *J. Am. Chem. Soc.* **2009**, *131*, 12792.
(20) Maji, T. K.; Mostafa, G.; Matsuda, R.; Kitagawa, S. *J. Am. Chem. Soc.* **2005**, *127*, 17152.
(21) Matsuda, R.; Kitaura, R.; Kitagawa, S.; Kubota, Y.; Kobayashi, T. C.; Horike, S.; Takata, M. *J. Am. Chem. Soc.* **2004**, *126*, 14063.
(22) Procopio, E. Q.; Linares, F.; Montoro, C.; Colombo, V.; Maspero, A.; Barea, E.; Navarro, J. A. R. *Angew. Chem., Int. Ed.* **2010**, *49*, 7308.
(23) Park, H. J.; Suh, M. P. *Chem.—Eur. J.* **2008**, *14*, 8812.
(24) Xiao, B.; Byrne, P. J.; Wheatley, P. S.; Wragg, D. S.; Zhao, X.; Fletcher, A. J.; Thomas, K. M.; Peters, L.; Evans, J. S. O.; Warren, J. E.; Zhou, W.; Morris, R. E. *Nature Chem.* **2009**, *1*, 289.
(25) Yan, Y.; Telepeni, I.; Yang, S.; Lin, X.; Kockelmann, W.; Dailly, A.; Blake, A. J.; Lewis, W.; Walker, G. S.; Allan, D. R.; Barnett, S. A.; Champness, N. R.; Schröder, M. *J. Am. Chem. Soc.* **2010**, *132*, 4092.
(26) Eddaoudi, M.; Moler, D. B.; Li, H.; Chen, B.; Reineke, T. M.; O'Keeffe, M.; Yaghi, O. M. *Acc. Chem. Res.* **2001**, *34*, 319.
(27) Serre, C.; Bourrelly, S.; Vimont, A.; Ramsahye, N. A.; Maurin, G.; Llewellyn, P. L.; Daturi, M.; Filinchuk, Y.; Leynaud, O.; Barnes, P.; Férey, G. *Adv. Mater.* **2007**, *19*, 2246.
(28) Kondo, A.; Noguchi, H.; Ohnishi, S.; Kajiro, H.; Tohdoh, A.; Hattori, Y.; Xu, W.-C.; Tanaka, H.; Kanoh, H.; Kaneko, K. *Nano Lett.* **2006**, *6*, 2581.
(29) Llewellyn, P. L.; Bourrelly, S.; Serre, C.; Filinchuk, Y.; Férey, G. *Angew. Chem., Int. Ed.* **2006**, *45*, 7751.
(30) Tanaka, D.; Nakagawa, K.; Higuchi, M.; Horike, S.; Kubota, Y.; Kobayashi, T. C.; Takata, M.; Kitagawa, S. *Angew. Chem., Int. Ed.* **2008**, *47*, 3914.
(31) Kitaura, R.; Seki, K.; Akiyama, G.; Kitagawa, S. *Angew. Chem., Int. Ed.* **2003**, *42*, 428.
(32) Coudert, F.-X.; Jeffroy, M.; Fuchs, A. H.; Boutin, A.; Mellot-Draznieks, C. *J. Am. Chem. Soc.* **2008**, *130*, 14294.
(33) Henke, S.; Schmid, R.; Grunwaldt, J.-D.; Fischer, R. A. *Chem.—Eur. J.* **2010**, *16*, 14296.
(34) Wu, H.; Reali, R. S.; Smith, D. A.; Trachtenberg, M. C.; Li, J. *Chem.—Eur. J.* **2010**, *16*, 13951.
(35) Xiao, B.; Byrne, P. J.; Wheatley, P. S.; Wragg, D. S.; Zhao, X. B.; Fletcher, A. J.; Thomas, K. M.; Peters, L.; Evans, J. S. O.; Warren, J. E.; Zhou, W. Z.; Morris, R. E. *Nature Chem.* **2009**, *1*, 289.
(36) Salles, F.; Maurin, G.; Serre, C.; Llewellyn, P. L.; Knofel, C.; Choi, H. J.; Filinchuk, Y.; Oliviero, L.; Vimont, A.; Long, J. R.; Férey, G. *J. Am. Chem. Soc.* **2010**, *132*, 13782.
(37) Sing, K. S. W.; Everett, D. H.; Haul, R. A. W.; Moscou, L.; Pierotti, R. A.; Rouquerol, J.; Siemieniewska, T. *Pure Appl. Chem.* **1985**, *57*, 603.
(38) Uemura, K.; Yamasaki, Y.; Komagawa, Y.; Tanaka, K.; Kita, H. *Angew. Chem., Int. Ed.* **2007**, *46*, 6662.
(39) Chen, B.; Liang, C.; Yang, J.; Contreras, D. S.; Clancy, Y. L.; Lobkovsky, E. B.; Yaghi, O. M.; Dai, S. *Angew. Chem., Int. Ed.* **2006**, *45*, 1390.
(40) Chun, H.; Dybtsev, D. N.; Kim, H.; Kim, K. *Chem.—Eur. J.* **2005**, *11*, 3521.
(41) Hong, S.; Oh, M.; Park, M.; Yoon, J. W.; Chang, J.-S.; Lah, M. S. *Chem. Commun.* **2009**, 5397.
(42) Farha, O. K.; Hupp, J. T. *Acc. Chem. Res.* **2010**, *43*, 1166.
(43) Yang, C.; Wang, X.; Omary, M. A. *Angew. Chem., Int. Ed.* **2009**, *48*, 2500.
(44) Llewellyn, P. L.; Horcajada, P.; Maurin, G.; Devic, T.; Rosenbach, N.; Bourrelly, S.; Serre, C.; Vincent, D.; Loera-Serna, S.; Filinchuk, Y.; Férey, G. *J. Am. Chem. Soc.* **2009**, *191*, 19002.
(45) Demessence, A.; Long, J. R. *Chem.—Eur. J.* **2010**, *16*, 5902.
(46) Choi, H.-S.; Suh, M. P. *Angew. Chem., Int. Ed.* **2009**, *48*, 6865.
(47) Hamon, L.; Llewellyn, P. L.; Devic, T.; Ghoufi, A.; Clet, G.; Guillerm, V.; Pirngruber, G. D.; Maurin, G.; Serre, C.; Driver, G.; Beek,

W. v.; Jolimaître, E.; Vimont, A.; Daturi, M.; Férey, G. *J. Am. Chem. Soc.* **2009**, *131*, 17490.
(48) Spek, A. L. *Acta Crystallogr., Sect. A* **1990**, *46*, 194.
(49) Nakamura, Y.; Aratani, N.; Osuka, A. *Chem. Asian J.* **2007**, *2*, 860.
(50) Sheldrick, G. M. *SHELX-97: Program for Crystal Structure Determination*; University of Gottingen: Germany, 1997.
(51) Kato, K.; Hirose, R.; Takemoto, M.; Ha, S.; Kim, J.; Higuchi, M.; Matsuda, R.; Kitagawa, S.; Takata, M. *AIP Conf. Proc.* **2010**, *1234*, 867.
(52) Hunter, B. A. *LHPM-Rietica Rietveld*, version 1.71; Australia, 1997.